Characterization and modeling of Fano resonances in chalcogenide photonic crystal membranes

Christian Grillet[1], Darren Freeman[2], Barry Luther-Davies[2], Steve Madden[2], Ross McPhedran[1], David J. Moss[1], Michael J. Steel[1],* and Benjamin J. Eggleton[1]

[1]Centre for Ultrahigh-bandwidth Devices for Optical Systems (CUDOS), School of Physics, University of Sydney, N SW 2006, Australia
[2]Centre for Ultrahigh-bandwidth Devices for Optical Systems (CUDOS), Laser Physics Centre, The Australian National University, Canberra, ACT 0200, Australia
**Also with the RSoft Design Group, Inc., 65 O'Connor Street, Chippendale, NSW 2008, Australia.*
grillet@physics.usyd.edu.au

Abstract: We demonstrate resonant guiding in a chalcogenide glass photonic crystal membrane. We observe strong resonances in the optical transmission spectra at normal incidence, associated with Fano coupling between free space and guided modes. We obtain good agreement with modeling results based on three-dimensional finite-difference time-domain simulations, and identify the guided modes near the centre of the first Brillouin zone responsible for the main spectral features.

OCIS codes: (260.5740) Resonance; (230.0230) Optical devices; (230.5440) Polarization-sensitive devices.

References and links

1. E. Yablonovitch, "Inhibited spontaneous emission in solid-state physics and electronics," Phys. Rev. Lett. **58**, 2059-2062 (1987).
2. S. John, "Strong localization of photons in certain disordered dielectric superlattices," Phys. Rev. Lett. **58**, 2486 (1987).
3. S. Noda, T. Baba, *Roadmap on photonic crystal*, (Springer, 2003).
4. C. Monat, C. Seassal, X. Letartre, P. Viktorovitch, P. Regreny, M. Gendry, P. Rojo-Romeo, G. Hollinger, E. Jalaguier, S. Pocas, and B. Aspar, "InP 2D photonic crystal microlasers on silicon wafer: room temperature operation at 1.55 μm," Electron. Lett. **37**, 764 (2001).
5. S. J. McNab, N. Moll, and Y. A. Vlasov, "Ultra-low loss photonic integrated circuit with membrane-type photonic crystal waveguides," Opt. Express **11**, 2927-2939 (2003).
6. X. Letartre, C. Seassal, C. Grillet, P. Rojo-Romeo, P. Viktorovitch, M. Le Vassor d'Yerville, D. Cassagne, and C. Jouanin, "Group velocity and propagation losses measurement in a single-line photonic-crystal waveguide on InP membranes" Appl. Phys. Lett. **79**, 2312 (2001).
7. H. M. Gibbs, *Optical Bistability: Controlling light with light* (Academic Press, Orlando, 1985).
8. D. A. B. Miller, "Optical Switching Devices: Some Basic Concepts," in *Optical Computing,* ed. B. S. Wherrett and F. A. P. Tooley, 55-70 (Adam Hilger, Bristol, 1989).
9. G. Lenz, B. J. Eggleton, C. K. Madsen, and R. E. Slusher, "Optical delay lines based on optical filters," IEEE J. Quantum Electron. **37**, 525 (2001).
10. Y. Ruan, W. Li, R. Jarvis, N. Madsen, A. Rode, and B. Luther-Davies, "Fabrication and characterization of low loss rib chalcogenide waveguides made by dry etching," Opt. Express **12**, 5140-5145 (2004).
11. E. Centeno and D. Felbacq, "Optical bistability in finite-size nonlinear bidimensional photonic crystals doped by a microcavity," Phys. Rev. B **62**, 7683-7686(R) (2000).
12. M. Soljacic, M. Ibanescu, S. G. Johnson, Y. Fink, and J. D. Joannopoulos, "Optimal bistable switching in nonlinear photonic crystals," Phys. Rev. E **66**, 055601(R) (2002).
13. M. F. Yanik, S. Fan, and M. Soljacic, "High-contrast all-optical bistable switching in photonic crystal microcavities," Appl. Phys. Lett. **83**, 2739-2741 (2003).
14. A. R. Cowan and J. F. Young, "Optical bistability involving photonic crystal microcavities and Fano line shapes," Phys. Rev. E **68**, 046606 (2003).
15. M. Notomi, A. Shinya, S. Mitsugi, G. Kira, E. Kuramochi, and T. Tanabe, "Optical bistable switching action of Si high-Q photonic-crystal nanocavities," Opt. Express **13,** 2678-2687 (2005).
16. F. Raineri, C. Cojocaru, P. Monnier, A. Levenson, R. Raj, C. Seassal, X. Letartre, and P. Viktorovitch, "Ultrafast dynamics of the third-order nonlinear response in a two-dimensional InP-based photonic crystal," Appl. Phys. Lett. **85**, 1880 (2004).

#9574 - $15.00 USD Received 18 November 2005; revised 30 December 2005; accepted 3 January 2006

17. F. Raineri, C. Cojocaru, R. Raj, P. Monnier, A. Levenson, C. Seassal, X. Letartre, and P. Viktorovitch, "Tuning a two-dimensional photonic crystal resonance via optical carrier injection " Opt. Lett. **30**, 010064 (2005).
18. V. N. Astratov, D. M. Whittaker , I. S. Culshaw, R. M. Stevenson, M. S. Skolnick, T. F. Krauss, and R. M. De La Rue, "Photonic band-structure effects in the reflectivity of periodically patterned waveguides," Phys. Rev. B **60**, 16255 (1999).
19. V. Lousse, W. Suh, O. Kilic, S. Kim, O. Solgaard, and S. Fan,"Angular and polarization properties of a photonic crystal slab mirror," Opt. Express **12**, 1575-1582 (2004).
20. U. Fano, "Effects of configuration interaction on intensities and phase shifts," Phys. Rev. **124**, 1866-1878 (1961).
21. D. Freeman, S. Madden, and B. Luther-Davies, "Fabrication of planar photonic crystals in a chalcogenide glass using a focused ion beam," Opt. Express **13,** 3079-3086 (2005).
22. D. Freeman et al, to be submitted.
23. S. Fan and J. D. Joannopoulos, "Analysis of guided resonances in photonic crystal slabs," Phys. Rev. B **65**, 235112 (2002).
24. T. Ochiai and K. Sakoda, "Dispersion relation and optical transmittance of a hexagonal photonic crystal slab," Phys. Rev. B **63**, 125107 (2001).

1. Introduction

Two-dimensional (2D) photonic crystal (PhC) slabs have become a promising class of dielectric structure for micro- and nano-photonics. Their ability to control light at the wavelength scale [1,2] has already led to impressive demonstrations of various passive devices [3] and micro-lasers [4]. These achievements are enabled by advanced technologies for patterning and etching materials such as silicon [5] or III-V semiconductors [6]. It is hoped that 2D PhC membranes will find utility in all-optical processors for ultra-fast and low power switching, optical logic gates, pulse regeneration, wavelength conversion, dispersion management and a variety of other applications [7-9].

Approaches for the enhancement of nonlinear optical effects have involved the development of new materials with stronger nonlinearities [10] and device structures that increase the optical intensity, by reducing the mode area or resonantly enhancing the fields [11-17]. In the present approach, a chalcogenide glass serves as the strongly third-order nonlinear material (100-1000× that of silica) and 2D PhCs make use of the large refractive index (2.4-3.0) to resonantly enhance the field. These glasses have low linear and nonlinear absorption losses compared to competing materials [15-16]. In addition to reducing the switching power requirements, the pure Kerr-like nonlinearities offer the potential for near instantaneous response times (<100 fs) and are only limited by the resonator Q-factor. This compares favorably to carrier-based nonlinear effects, as exploited in silicon [15] or III-V-based devices [16], which rely on dissipation to occur after switching, limiting the response time to tens of picoseconds.

In this work, we experimentally characterize and numerically model strong optical resonances in a chalcogenide glass PhC membrane. We observe strong guided resonances [18-19], also called "Fano" resonances in analogy with atomic physics [20], in the optical transmission spectrum at normal incidence. These arise from photonic states near the center of the first Brillouin zone (in-plane wave-vector equal to zero), and the structure can be thought of as a resonant dielectric mirror. We achieve good agreement using 3D finite-difference time-domain (FDTD) simulations. We have identified the guided modes responsible for the resonances and show their field distributions. This work is the result of recent advances in chalcogenide glass photonic crystal membrane fabrication by focused ion beam (FIB) milling [21], and Fano resonance probing techniques [18].

2. Fabrication

We restrict our attention now to a particularly successful device whose fabrication will be described in detail elsewhere [22]. It consists of a free-standing membrane of chalcogenide glass perforated with a triangular lattice of air holes. The chalcogenide glass film, approximately 300 nm thick, having the refractive index ~2.7 and composition $Ge_{33}As_{12}Se_{55}$ ("AMTIR-1"), was deposited using ultra-fast pulsed laser deposition (UFPLD) onto a 30 nm

#9574 - $15.00 USD Received 18 November 2005; revised 30 December 2005; accepted 3 January 2006

thick Si_3N_4 (silicon nitride) membrane. The supporting membrane was fabricated by wet etching the backside of a nitrided Si wafer. The square windows thus formed had a free-standing aperture of approximately 130 μm. Subsequently a thin Au coating was applied to both sides and a Ga^+ FIB was used to mill cylindrical holes into the film from the nitride side. The beam first had to penetrate the relatively robust nitride layer before milling the softer glass, so as to block the unwanted ions and form nearly vertical sidewalls. This greatly reduced the sculpting of the upper glass surface by the low intensity beam pedestal compared to earlier work [21]. A high-resolution scanned electron micrograph of a similar structure is shown in Fig. 1, imaged from the glass side. The device under test was not imaged in this way because we have observed electron-induced refractive index changes in the past. Finally the Au was stripped for testing. The lattice had a period of 1 μm, with nominally 250 nm radius holes, over a hexagonal region having 115 periods in the Γ-K direction. The sidewall roughness is very low in these structures, estimated to be <3 nm in our previous work [21]. The nearly cylindrical holes had sharp edges where they met the surface of the membrane.

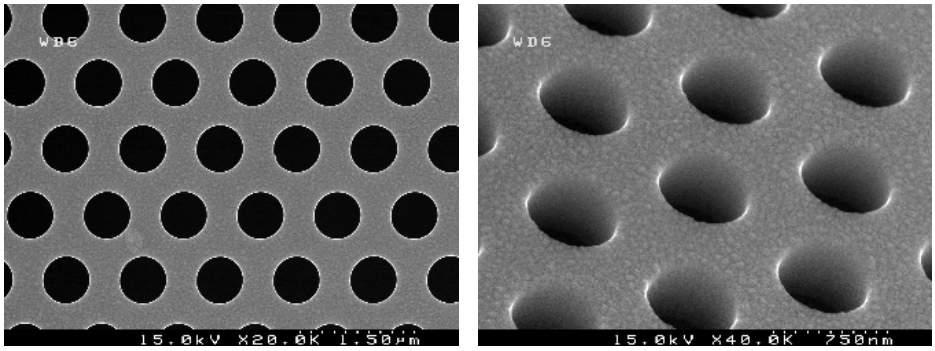

Fig. 1. Electron micrographs of a chalcogenide glass photonic crystal membrane imaged at 0° and 45°. The Au coating creates the visible surface texture.

3. Experimental set-up

The structure thus obtained was experimentally characterized by measuring the optical transmission spectrum at normal incidence (Fig. 2). We limit discussions to normal incidence (θ=0°) where in theory results are independent of polarization. We created a super-continuum source by passing 1.5 kW, 10 ps pulses from a mode-locked Nd:YVO_4 laser (1064 nm) through a 20 m long section of PhC fiber with zero dispersion at 1040 nm. The resulting single-mode beam had significant power from below 600 nm to above 1700 nm, and after attenuation and polarization, it was focused on the structure via a microscope objective to a spot size of approximately 30 μm. The transmitted light was collected by a fiber (single-mode at 1550 nm) placed in proximity to the membrane, and recorded using an optical spectrum analyzer. The spectra were normalized against free-space transmission in the same configuration.

#9574 - $15.00 USD Received 18 November 2005; revised 30 December 2005; accepted 3 January 2006

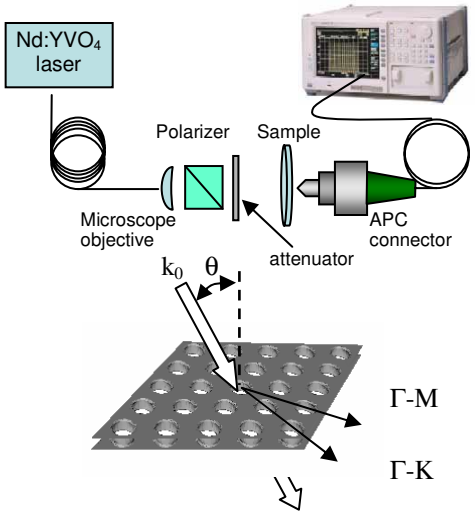

Fig. 2. Experimental setup used to measure the optical transmission spectrum.

4. Experimental and modeling results

Resonances due to coupling to resonant photonic crystal guided modes are observed in transmission when the phase matching condition is satisfied (Fig. 2).

$$|k_0| \sin\theta = |\beta_{//} + \kappa_G| \tag{1}$$

where k_0 is the wave vector of the incident light, θ is the angle of incidence, $\beta_{//}$ is the wave vector component in the plane of the slab and κ_G is any reciprocal lattice vector.

The transmission spectrum at normal incidence for a beam linearly polarised along the Γ-M direction is shown in Fig. 3 (logarithmic scale), where we observe strong resonances with transmission suppressed by as much as 42 dB.

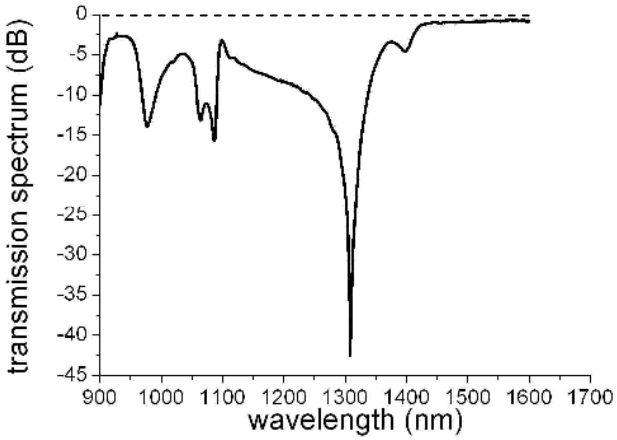

Fig. 3. Experimental optical transmission spectrum on a logarithmic scale. Radius r = 250 nm.

#9574 - $15.00 USD Received 18 November 2005; revised 30 December 2005; accepted 3 January 2006

These sharp, asymmetric features in the spectra are the Fano resonances, which can be understood as the interference between the directly transmitted waves (as governed by the Fabry-Pérot response of the slab) and the waves emanating from the excited PhC leaky modes [23].

Figure 4 shows the experimental optical transmission spectrum (linear scale) together with simulated results, showing satisfactory agreement. The theoretical spectrum was calculated using a 3D finite-difference time-domain (FDTD) method [23], with a domain that included a single unit cell of the crystal. The calculations account for the thin Si_3N_4 support membrane as well as the measured material dispersion of the chalcogenide through a Lorentzian approximation (only one resonance term is used for this calculation):

$$\varepsilon(\omega) = \varepsilon_\infty + \frac{\Delta\varepsilon}{a(i\omega)^2 - b(i\omega) + c} \tag{2}$$

where ε_∞ is the value of ε in the limit of infinite frequency (ε_∞ = 3.7), $\Delta\varepsilon$ is the resonator strength ($\Delta\varepsilon$ = 592), and *a*, *b*, *c* are fitting coefficients. In a Lorentzian approximation, *a* is set to one, *b* (= 0.05) is related to the damping factor and *c* (= 197.4) is related to the resonant frequency. The following parameters were used for this calculation: triangular lattice of air holes, lattice constant 1 μm and radius 250 nm, in chalcogenide slab thickness 300 nm, Si_3N_4 support membrane thickness 100 nm with an index 1.9. The skewed rectangular simulation volume had Bloch periodic boundary conditions imposed on the four out-of-plane surfaces, while the two surfaces parallel to the slab had perfectly matched layer (PML) absorbers.

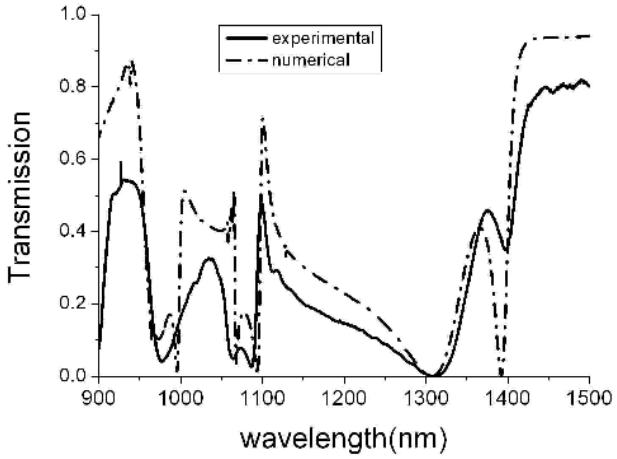

Fig. 4. Experimental and theoretical transmission spectra compared on a linear scale. Radius r = 250nm.

To produce the free-space excitation, an infinite plane-wave field was launched from above, having a Gaussian pulse temporal envelope. A monitor point was inserted to record the time-domain fields on both sides of the slab. Spectra were obtained by Fourier transforming the resulting waveforms and were normalized appropriately. The agreement between theory and experiment is particularly noteworthy, considering that the experimental beam divergence (half angle divergence about 1.5 degree) and the effect of the finite size of the beam and PhC region are not taken into account in the modeling.

To identify which guided modes were responsible for the Fano resonances, we present the band diagram for the PhC in Fig. 5, along with the electric field intensity distributions of the relevant modes.

#9574 - $15.00 USD Received 18 November 2005; revised 30 December 2005; accepted 3 January 2006

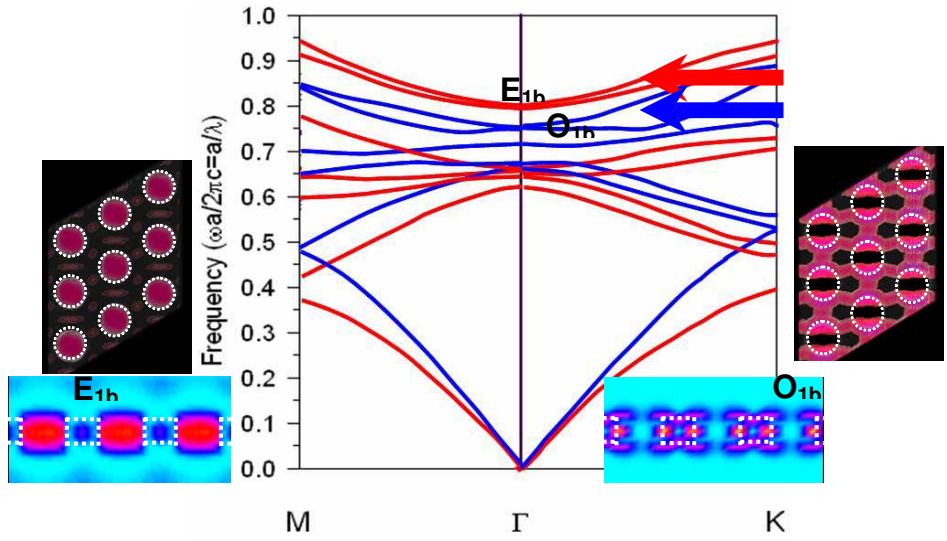

Fig. 5. Photonic band diagram obtained by 3D plane wave calculations along with electric field intensity distributions of the modes responsible for the main Fano resonances. High intensity distribution regions are in red.

The dispersion of the guided modes was obtained from a 3D plane-wave band structure method, with a supercell approach (RSoft BandSOLVE) that does not include material dispersion or the thin nitride support membrane. The blue and red lines represent odd and even modes, with respect to the slab plane. The two main spectral features are associated with the modes we denote E1b (even) and O1b (odd) modes at the Γ-point on the band diagrams. The bandstructure calculation is an idealization of the true problem, so the predicted frequency of these modes in Fig. 5. is inconsistent with the results in Fig. 4. Hence we made this identification as follows. We performed a sequence of FDTD simulations, removing first the dispersion and then the Si_3N_4 layer. We tracked the movement of the two resonances from one simulation to the next. Their location in the final idealized FDTD simulation matched perfectly to the band structure results. Both E1b and O1b are doubly degenerate modes with complementary symmetry properties that allow them to couple to free-space [24].

From Fig. 4 and 5 we see that the resonance at 1.4 μm arises from coupling to the O1b mode, whilst the low-Q resonance resulting in the wide transmission dip down to –42 dB around 1.3 μm is related to the strong coupling of the E1b mode to free-space. This is confirmed by the electric intensity distribution where we can see that E1b concentrates most of its electric energy in the air region. Finally, the observed resonances at 1.1 μm and 1.0 μm are also found to be in the same locations in the 3D FDTD results and are related to coupling to higher order modes. As noted by Ochiai *et al.* [24], the coupling between O1b and E1b modes is forbidden by group theoretic arguments even in the case where mirror symmetry with respect to the slab plane is broken as in our structure. The response of our structure should therefore be similar to that of a symmetric membrane, and it allows us to identify the modes as even- or odd-like.

#9574 - $15.00 USD Received 18 November 2005; revised 30 December 2005; accepted 3 January 2006

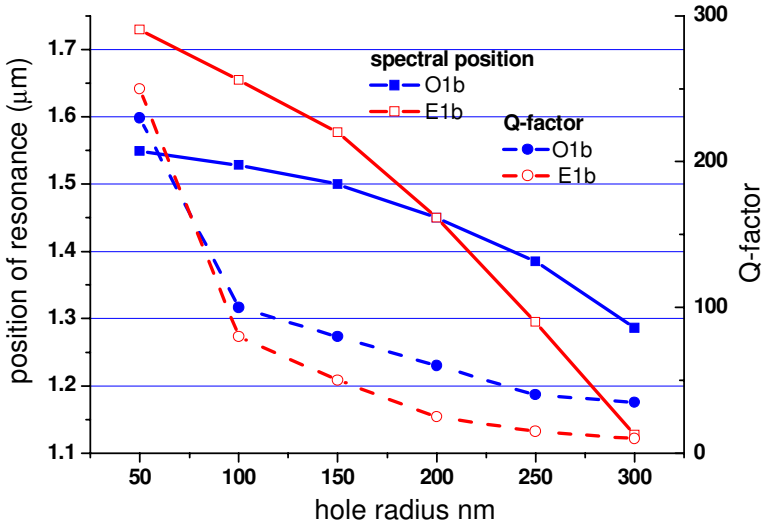

Fig. 6. Influence of holes radii on the spectral position of E1b and O1b and their related Qfactor.

In Fig. 6 we have plotted the influence of holes radii on the spectral position of E1b and O1b and their related Q-factor. As the radius increases (from 50nm to 300nm), we notice that the E1b and O1b modes are shifted towards shorter wavelength, E1b faster than O1b. The two modes overlap for r = 200nm. For any hole radius larger than 200nm E1b becomes shorter in wavelength than O1b. At the same time, the Q-factors associated with the guided resonances, become smaller as the radii increase. As expected the Q-factor associated to E1b decreases faster than O1b. The E1b mode is related to a TE like mode, where the eletric field is mainly lying in the slab and should thus be particularly sensitive to discontinuity in the plane and consequently sensitive to structural parameters changes. Figure 7 confirms this trend: it shows the simulated results together with the experimental optical transmission spectrum (linear scale) for a nominal radius hole of 300 nm. We recognize at 1.15 µm the resonance related to the strong coupling of the E1b mode to free space. Note that the experimental beam divergence limits the measured Q-factors of experimental features. This then explains many of the quantitative differences between theory and experiment in Fig. 4 and Fig. 7, including the fact that O1b, due to its higher Q, appears as only a relatively weak dip, "smeared" by the beam divergence and lattice irregularities. Nonetheless, the agreement in the positions of the resonances is remarkable and emphasizes the quality of the structure: even a TE-like mode such as E1b, which should be particularly sensitive to disorder (inhomogeneity in hole radii and/or in period), matches the numerical predictions.

#9574 - $15.00 USD Received 18 November 2005; revised 30 December 2005; accepted 3 January 2006

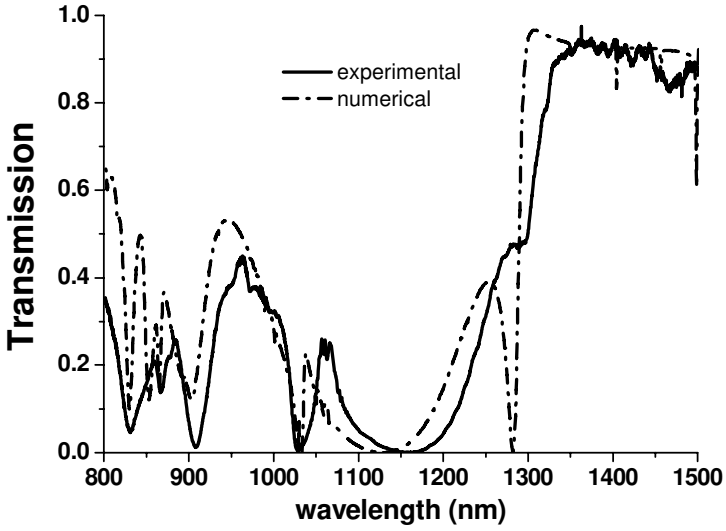

Fig. 7. Experimental and theoretical transmission spectra compared on a linear scale. Radius r = 300nm.

5. Conclusion

In conclusion, we have observed Fano resonances in the optical transmission spectrum of a chalcogenide glass photonic crystal membrane. We have achieved reasonable agreement between experiment and simulation based upon a three-dimensional finite-difference time-domain method. We demonstrate, for the first time, the suppression of optical transmission by over 40 dB, the strongest reported so far and a remarkable result for a dielectric structure just 330 nm thick. The resulting insights gained will allow further work towards engineering very sharp resonances and, combined with the large intrinsic nonlinearity of the chalcogenide glasses, should allow the demonstration of optical bistability in a PhC mirror.

Acknowledgments

This work was produced with the assistance of the Australian Research Council (ARC). CUDOS (the Centre for Ultrahigh-bandwidth Devices for Optical Systems) is an ARC Centre of Excellence. We thank Andrei Rode for depositing the film, Maryla Krolikowska for preparation of the membranes, and ANU Electron Microscopy Unit for use of the FIB.

#9574 - $15.00 USD Received 18 November 2005; revised 30 December 2005; accepted 3 January 2006